Invited Paper

Nonlinear dynamics of optical frequency combs

Stefan Wabnitz[a,d], Tobias Hansson[b], François Leo[c], Iolanda Ricciardi[d], Maurizio De Rosa[d], Stéphane Coen[e], and Miro Erkintalo[e]

[a]Dipartimento di Ingegneria dell'Informazione, Università di Brescia, via Branze 38, 25123 Brescia, Italy
[b]INRS-EMT, 1650 Blvd. Lionel-Boulet, Varennes, Québec J3X 1S2, Canada
[c]OPERA-photonics, Université libre de Bruxelles, 50 Avenue F. D. Roosevelt, CP 194/5, B-1050 Bruxelles, Belgium
[d]CNR-INO, Istituto Nazionale di Ottica, Via Campi Flegrei 34, 80078 Pozzuoli (NA), Italy
[e]The Dodd-Walls Centre for Photonic and Quantum Technologies, Department of Physics, The University of Auckland, Auckland 1142, New Zealand

ABSTRACT

We discuss recent advances in the modelling of optical frequency comb generation in quadratic and cubic microresonators. Different time domain models are presented and compared, and their solutions are analysed by numerical methods.

Keywords: Optical Frequency Combs, Microresonators, Nonlinear Optics, Second Harmonic Generation, Optical Parametric Oscillation

1. INTRODUCTION

One of the most promising applications of nonlinear integrated optics is that of nonlinear microresonator based optical frequency comb light sources. Optical comb sources are characterized by a spectrum comprising many equally spaced frequency components, and have a wide range of technological applications. Although commercial comb generators are based on mode-locked lasers and fiber supercontinuum generation, nonlinear integrated optics provides a low-cost and chip-scale alternative, which is based on using a relatively low-power CW pump laser coupled into a high-Q microresonator.[1] So far, microresonator frequency combs have mostly exploited materials with third-order Kerr nonlinearity, which permits to generate successive comb lines with a spacing equal to the resonator free-spectral range or its multiples, by the mechanism of cascade four-wave mixing.[2–4]

Modelling of the temporal dynamics of microresonator frequency combs can be greatly simplified by means of a single partial differential equation approach, in analogy with the case of other coherently driven Kerr spatially diffractive or temporally dispersive nonlinear cavities. In order to lower the threshold pump power, and to extend the spectral range of frequency comb generation, for example into the visible or mid-infrared, while still using near-infrared CW laser pumps, the use of quadratic nonlinear cavities has been recently proposed.[5,6] Remarkably, efficient quadratic microresonator frequency comb sources are found to operate close to the phase-matching condition for the underlying quadratic processes.

A single time-domain partial differential equation with an effective delayed third-order nonlinearity was recently derived for describing, with good accuracy, the dynamics of quadratic frequency comb generation by means of intra-cavity second-harmonic generation. Analogous equations are obtained under different phase-matching conditions corresponding to, e.g., optical parametric oscillation. In more general situations where multiple phase-matched wave mixing processes are present, and the frequency combs generated around the interacting waves over multiple octaves overlap, numerical modeling may usefully exploit a single envelope equation approach. This formalism permits to naturally include the simultaneous presence of both quadratic and cubic nonlinearities in the modeling of the comb dynamics. In the case of semiconductor based microresonators, such as silicon

Further author information: (Send correspondence to S. Wabnitz)
S. Wabnitz.: E-mail: stefan.wabnitz@unibs.it

Integrated Optics: Physics and Simulations III, edited by Pavel Cheben, Jiří Čtyroký, Iñigo Molina-Fernández, Proc. of SPIE Vol. 10242, 102420G · © 2017 SPIE
CCC code: 0277-786X/17/$18 · doi: 10.1117/12.2264579

microrings, the single envelope equation for the optical field should additionally be coupled with the equation describing the dynamics of carrier population.

2. CUBIC FREQUENCY COMBS

The evolution of the slowly-varying electric field envelope $A(t,\tau)$ (in units of $[\sqrt{W}]$) inside a cubic nonlinear microresonator may be modeled by means of a map in the time domain. In a reference frame that travels with the group velocity of the pump, nonlinear and dispersive propagation in the m-th roundtrip (in a ring of length L) is described by the lossy nonlinear Schrödinger equation (NLSE)

$$\frac{\partial A_m}{\partial z} = \left[-\alpha_\mathrm{i} + iD\left(i\frac{\partial}{\partial \tau}\right)\right] A_m + i\gamma |A_m|^2 A_m. \tag{1}$$

where z is the distance along the ring circumference, τ is a *fast time* variable that permits to describe the intra-cavity field profile, α_i is the distributed linear loss coefficient, and γ is the Kerr nonlinearity coefficient. Dispersion is included in the model, to all orders, through the operator $D_(x) = \sum_{l\geq 2}(k^{(l)}/l!)x^l$, where $k^{(l)} = d^l k/d\omega^l|_{\omega_0}$ are dispersion coefficients obtained by a Taylor series expansion of the propagation constant. The map is completed by requiring that the recirculating field should satisfy the cavity boundary condition

$$A_{m+1}(0,\tau) = \sqrt{1-\theta}A_m(L,\tau)e^{-i\delta} + \sqrt{\theta}A_\mathrm{in}, \tag{2}$$

where θ is the power transmission coefficient of the coupler used to inject the CW driving field A_in, and $\delta = 2\pi l - \phi_0$ is the phase detuning of the driving field with respect to the closest linear resonance (with order l). Whenever the variation of the pulse envelope between successive round trips remains small (which is the case for a high-finesse cavity such as that of an optical microresonator), one may average the so-called Ikeda map of Eq. (1) and Eq. (2) over the roundtrip length L, to obtain the driven-damped NLSE:[7,8]

$$t_\mathrm{R}\frac{\partial A(t,\tau)}{\partial t} = \left[-\alpha - i\delta + iLD\left(i\frac{\partial}{\partial \tau}\right)\right] A + i\gamma L|A|^2 A + \sqrt{\theta}\, A_\mathrm{in}. \tag{3}$$

Here, t_R is the cavity roundtrip time, and $\alpha = (\alpha_\mathrm{i}L + \theta)/2$ describes the total cavity losses. The continuous variable t is a *slow time* that measures the evolution of the field envelope over several roundtrips. The cavity boundary conditions impose the field to be $\tau-$periodic with period t_R, i.e., $A(t,\tau) = A(t,\tau + t_R)$. When neglecting higher-order dispersion terms ($k^{(l)} = 0$ for $l > 2$), Eq. (3) is formally identical with the so-called Lugiato-Lefever equation (LLE) that was introduced to describe pattern formation in spatially diffractive Kerr cavities.[9] Essentially the same equation also describes coherently-driven passive optical fiber cavities in the limit of a dense mode spectrum.[7,10]

The advantage of using the cavity averaged Eq. (3) for describing optical frequency comb generation in a microresonator is twofold. On the one hand, the use of Eq. (3) generally permits a faster numerical solution than the Ikeda map of Eq. (1) and Eq. (2), because in some instances the integration step can be even larger than the cavity length L. More importantly, Eq. (3) permits a much simplified analytical study of the modulation instability (MI) of the CW cavity solutions,[7,12] and it leads to approximate analytical solutions, such as the cavity solitons, by means of standard perturbation methods of the NLSE.[13]

It should be noted, however, that in situations where the intracavity power reaches high values, the solution of the more general map of Eq. (1) and Eq. (2) leads to interesting phenomena which cannot be described by the LLE (3) approach.[11,14] The left panel of Fig. 1 compares the dependence on pump intensity of the CW solution of the intra-cavity field for the map (orange solid) and the averaged NLSE (blue dashed). As can be seen, the map predicts that very high values of the intra-cavity intensity can be reached even for relatively moderate levels of the pump intensity. A more striking difference is observed in the MI gain of the CW solutions, as illustrated by the right panel of Fig. 1: here in addition to MI bands the gain profile also describes the onset of period-2 (P2) instabilities.[11,14]

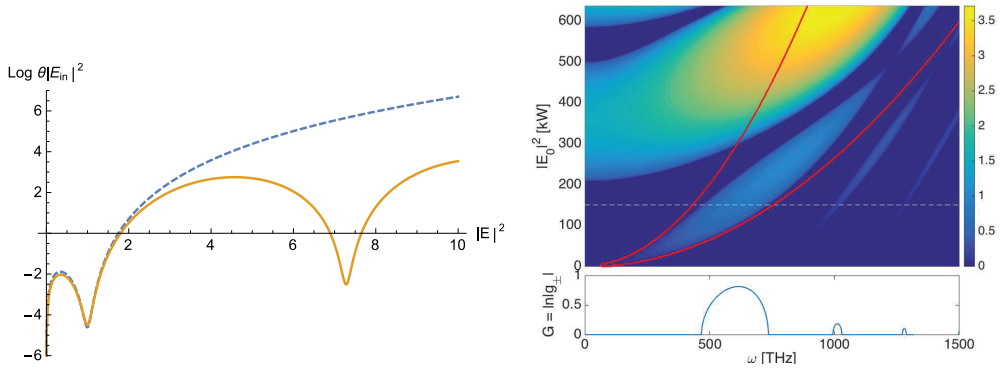

Figure 1. Left: Comparison of pump dependence on the intracavity power for multi-valued stationary continuous wave solutions of the LLE (blue dashed) and the Ikeda map (orange solid). Parameters $\alpha = \theta = 0.1$ and $\gamma = L = P_{in} = \delta = 1$. Right: Parametric instability tongues of the Ikeda map for anomalous dispersion. The red contour shows the predicted range of MI for the LLE. Below a cross section corresponding to the dashed line is shown with alternating CW-MI/P2-MI gain bands. Parameters: $\gamma = 25$ W^{-1}km^{-1}, $L = 2\pi \times 40$ μm, $\mathcal{F} = 10^6$, $\beta_2 = -40$ ps^{2}km^{-1} and $\delta_0 = 0$.[11]

The existence of multistable CW solution branches for the map as seen in the left panel of Fig. 1 also leads to the appearance of multistable cavity solitons. Figure 2 shows two examples of cavity solitons that are obtained for exactly the same values of the pump driving and cavity parameters. Although the cavity soliton shown in the left panel of Fig. 2 can be well approximated by the corresponding solution of the LLE (3), the cavity soliton shown in the right panel of Fig. 2 has no counterpart in the cavity averaged model, and it is characterized by a much higher peak power: hence it has been named a *super cavity soliton*.[11]

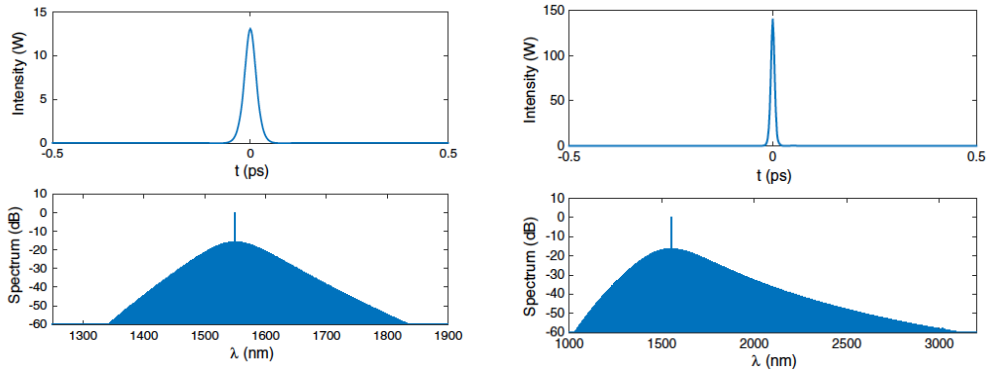

Figure 2. Left: LLE type cavity soliton. Simulation of Ikeda map Eqs.(11-12), with parameters $\alpha = \theta = 0.01$, $\gamma = 100$ W^{-1}m^{-1}, $L = 0.1$ mm, $P_{in} = 1$ W, $FSR = 100$ GHz, $\beta_2 = -500$ ps^2/km and $\delta_0 = 0.6$; Right: Stationary super cavity soliton, using the exact same parameters as in the left panel, except for different initial conditions.[11]

3. QUADRATIC FREQUENCY COMBS

Similar to the case of a cubic nonlinear microresonator described in Sec. 2, the generation of optical frequency combs from a quadratic microresonator can also be modeled by means of a map in the time domain. This map involves propagation equations for the fundamental field (FF) and the second harmonic (SH) field, coupled with appropriate boundary conditions, which describe coherent pump injection, and link the fields between successive roundtrips. Let us define with $A_m(z,\tau)$ and $B_m(z,\tau)$ the slowly-varying envelopes of the electric field of the FF (ω_0) and the SH ($2\omega_0$) field, respectively. In a reference frame that travels with the group velocity of the FF, nonlinear and dispersive propagation in the m-th roundtrip (in a ring of length L) is described by the following equations,[15–18]

$$\frac{\partial A_m}{\partial z} = \left[-\frac{\alpha_{c1}}{2} + iD_1\left(i\frac{\partial}{\partial \tau}\right)\right] A_m + i\kappa B_m A_m^* e^{-i\Delta k z}, \tag{4}$$

$$\frac{\partial B_m}{\partial z} = \left[-\frac{\alpha_{c2}}{2} - \Delta k'\frac{\partial}{\partial \tau} + iD_2\left(i\frac{\partial}{\partial \tau}\right)\right] B_m + i\kappa A_m^2 e^{i\Delta k z}. \tag{5}$$

Dispersion is described now by the two different operators $D_{1,2}(x) = \sum_{l\geq 2}(k_{1,2}^{(l)}/l!)x^l$, with $k_{1,2}^{(l)} = d^l k/d\omega^l|_{\omega_0,2\omega_0}$. In Eqs. (4-5) we have defined $\Delta k = 2k_1 - k_2$ as the wave-vector mismatch for the SHG process, while $\Delta k' = k_2^{(1)} - k_1^{(1)}$ is the group-velocity mismatch between the fundamental and second harmonic fields. The nonlinear coefficient is given by $\kappa = \sqrt{8}\omega_0\chi_{\text{eff}}^{(2)}/\sqrt{c^3 n_1^2 n_2 \epsilon_0}$, where $\chi_{\text{eff}}^{(2)}$ is the effective second-order susceptibility, c the speed of light, $n_{1,2}$ are the refractive indices evaluated at the FF and SH field frequencies, respectively, and ϵ_0 is the vacuum permittivity. Additionally, the absorption coefficients for each of the two fields are $\alpha_{c1,2}$, respectively.

3.1 Intracavity SHG

For the case of intra-cavity SHG, the map is completed by the two cavity boundary conditions,

$$A_{m+1}(0,\tau) = \sqrt{1-\theta_1}A_m(L,\tau)e^{-i\delta_1} + \sqrt{\theta_1}A_{\text{in}}, \tag{6}$$

$$B_{m+1}(0,\tau) = \sqrt{1-\theta_2}B_m(L,\tau)e^{-i\delta_2}. \tag{7}$$

where $\theta_{1,2}$ are power coupling coefficients, $\delta_{1,2}$ is the phase detuning for each of the two fields, and the resonator is driven at the FF by the external cw field A_{in}.

The map Eqs. (4-7) can be used to model the evolution of the FF and SH field, but once again - as in Sec. 2, considerable simplification results by using the mean-field theory. We suppose first the SH field to be slaved to the FF, and that the FF evolves slowly during each roundtrip. By assuming the coupling coefficient $\theta_1 \ll 1$ and the detuning $\delta_1 \ll 1$, and by averaging Eqs. (4-5) over the resonator length L,[7] one obtains the following mean-field equation

$$t_R\frac{\partial A(t,\tau)}{\partial t} = \left[-\alpha_1 - i\delta_1 + iLD_1\left(i\frac{\partial}{\partial \tau}\right)\right] A - \rho A^*[A^2(t,\tau)\otimes I(\tau)] + \sqrt{\theta_1}A_{\text{in}}, \tag{8}$$

where $\alpha_1 = (\alpha_{c1}L + \theta_1)/2$ is the FF round-trip loss, $\otimes$ denotes convolution and $I(\tau) = \mathscr{F}^{-1}[\hat{I}(\Omega)]$ (where $\mathscr{F}[\cdot] = \int_{-\infty}^{\infty}\cdot\, e^{i\Omega\tau}\,\mathrm{d}\tau$ denotes Fourier transformation) is a nonlinear response function. As can be seen, the mean-field Eq. (8) for a quadratic cavity exhibits an effective third-order non-instantaneous nonlinearity, in analogy with the case of a delayed Raman response[19] and other non-instantaneous nonlinear Schrödinger models.[20] However, contrary to those models, this is a coherent nonlinear process, since the square of the FF, rather than its intensity, is involved. The nonlinear response function $I(\tau)$ and the nonlinear coefficient ρ take different forms, depending on whether the SH field is also resonant in the cavity or not, as we shall see in the next subsections.

3.2 Singly resonant SHG

Figure 3 provides a schematic illustration of optical frequency comb generation around the FF and SH field in a singly resonant quadratic microresonator.[16,18] As can be seen, the FF driving field A_{in} is coupled into the microring and recirculates in the cavity, whereas the SH field that is generated during propagation through the ring is fully out-coupled at each round-trip. This means that $\theta_2 = 1$, hence $B_{m+1}(0,\tau) = 0$ in Eq. (7). In this case, the nonlinear response function of Eq. (8) reads as[16,18]

$$\hat{I}(\Omega) = \frac{1}{L^2}\int_0^L\int_0^z e^{(\hat{k}-i\Delta k)(z-z')}\,dz'dz = \frac{1-e^{-ix}-ix}{x^2}, \tag{9}$$

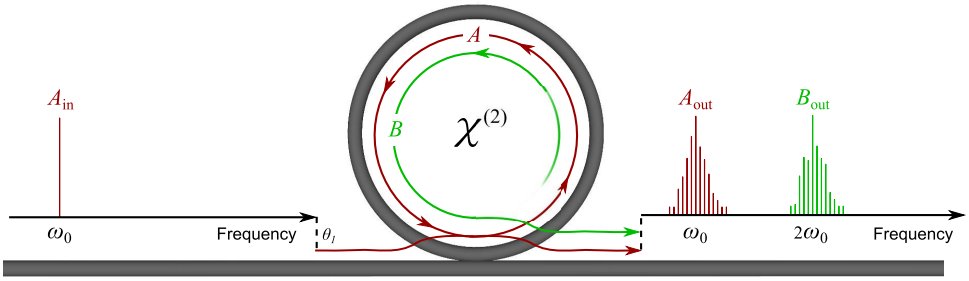

Figure 3. Schematic of singly resonant SHG in microring.

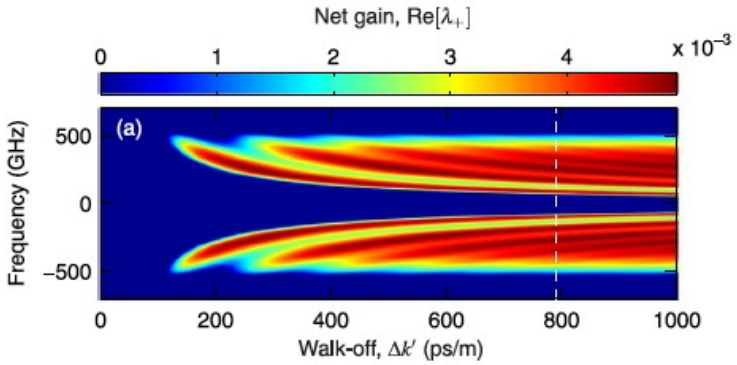

Figure 4. MI gain for a singly resonant SHG system as a function of frequency and walk-off.[16]

with $x(\Omega) = [\Delta k + i\hat{k}(\Omega)]L$, and $\hat{k}(\Omega) = -\alpha_{c2}/2 + i[\Delta k'\Omega + \hat{D}_2(\Omega)]$ (the hat denotes here a function defined in the Fourier domain). Moreover, $\rho = (\kappa L)^2$.

The use of a single cavity averaged Eq. (8) strongly facilitates the study of the CW solutions for the intracavity fundamental field intensity, and its MI gain profile. Figure 4 shows an example of the MI gain spectrum as a function of the walk-off parameter $\Delta k'$. From this figure, it is clear that there is no MI for $\Delta k' = 0$. On the other hand, Fig. 4 shows that MI does occur for sufficiently large values of the walk-off. This can be explained by noting that a large $\Delta k'$ causes sum-frequency processes to be heavily phase-mismatched, thereby reducing the level of nonlinear losses seen sub-harmonic field around the FF at ω_0.[16,18]

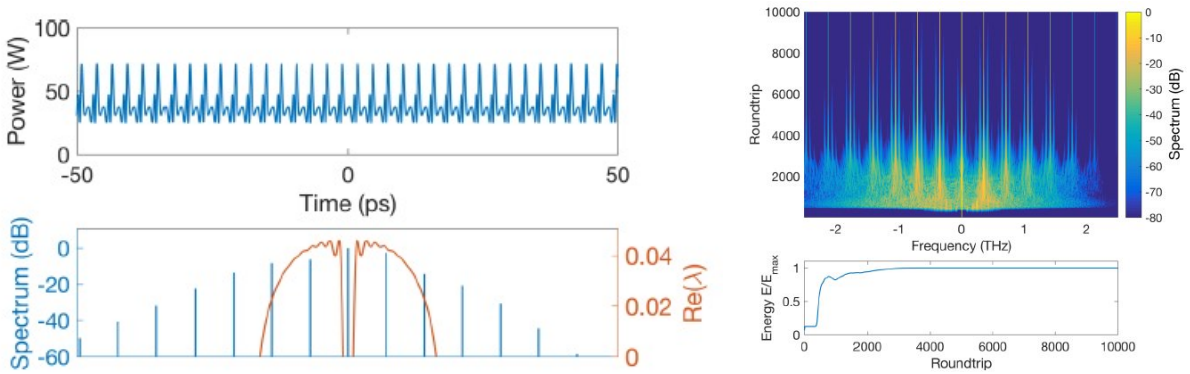

Figure 5. Spectral evolution of the fundamental field (upper right panel). Top left plot shows temporal profile, below it is shown the final spectrum and the initial MI growth rate, while the bottom right plot shows evolution of the dimensionless intracavity energy.[18]

The cavity MI gain shown in Fig. 4 leads to the initial growth of primary sidebands around the FF. The successive temporal dynamics of the comb generation process is illustrated in Fig. 5. Here we numerically solved Eq. (8) with a fixed value of the cavity detuning, and show the evolution of the intra-cavity spectrum over 10 000 roundtrips (~ 20 μs). The top left panel of Fig. 5 shows the final temporal pattern, and below we show the corresponding comb spectrum, alongside with the MI gain profile.[18] The comb evolution shown in the top right panel of Fig. 5 shows that the MI of the CW pump initially leads to a broad spectrum involving many cavity modes with the fundamental spacing of a single free-spectral-range (FSR). After roughly 2 000 roundtrips, a few modes spaced by 39 FSRs become phase-locked and start to dominate the spectra. Later on additional harmonics further away also lock, until a stationary frequency comb is reached. This comb represents a maximum for the intracavity energy (bottom right panel of Fig. 5).

3.3 Doubly resonant SHG

The process of optical frequency comb generation in a doubly resonant microresonator is illustrated in Fig. 6. As can be seen, in this case both the FF and the SH field recirculate inside the cavity. This means that $\theta_2 \ll 1$, hence $B_{m+1}(0,\tau) \neq 0$ in Eq. (7). In such a situation, the nonlinear response function of Eq. (8) can be written as[17]

$$\hat{I}(\Omega) = \frac{1}{\alpha_2 + i\delta_2 - i\Delta k' L\Omega - i\frac{k_2'' L}{2}\Omega^2}. \tag{10}$$

Moreover, $\rho = (\kappa L)^2 \mathrm{sinc}^2(\xi)$, where $\xi = \Delta k L/2$. By assuming phase-matched intra-cavity SH generation (i.e., $\Delta k = \xi = 0$, and $\delta_2 = 2\delta_1$), one may calculate from Eq. (8) the cavity MI gain as a function of frequency Ω and dimensionless walk-off $d = \Delta k' \left[2L/(\alpha_1 |k_1''|)\right]^{1/2}$ as shown in Fig. 7.

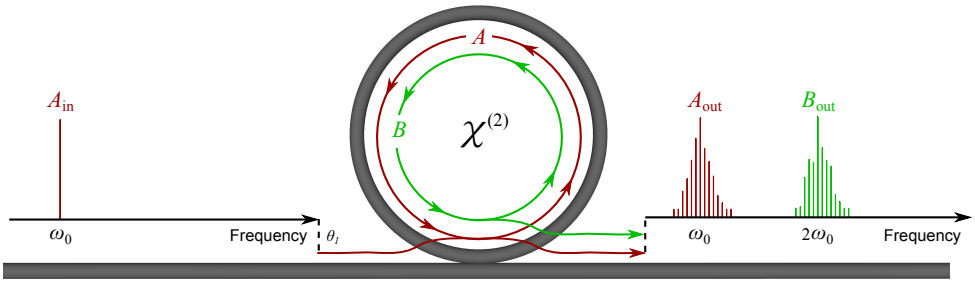

Figure 6. Schematic of doubly resonant SHG in microring.

In contrast with the case of singly resonant SH generation of Sec. 3.2,[16] in the doubly resonant case MI may also arise with zero walk-off, i.e., $d = 0$. As d increases, however, the MI gain quickly reduces and eventually disappears altogether. For sufficiently large walk-off values ($|d| \gg 1$) there is a new branch of MI, which is responsible for frequency comb generation.[17]

Similar to the case discussed for a singly resonant cavity in Sec. 3.2, the long-term evolution of an MI unstable pump field can result in frequency comb generation. In Fig. 8 we show an example of numerically computed temporal and spectral profiles associated with stable and fully coherent frequency combs that are generated around the FF and SH frequencies, respectively. As can be seen, in the time-domain the intra-cavity fields are composed of three, periodically-spaced temporal structures, corresponding to a frequency comb with $3 \times$ FSR spacing.[17]

4. CUBIC AND QUADRATIC COMBS

For describing ultra-broadband fields with multiple harmonics, or whenever the fundamental and second harmonic fields are partially overlapping, it is necessary to develop a more general model than what is described in Sec. 3.[21]

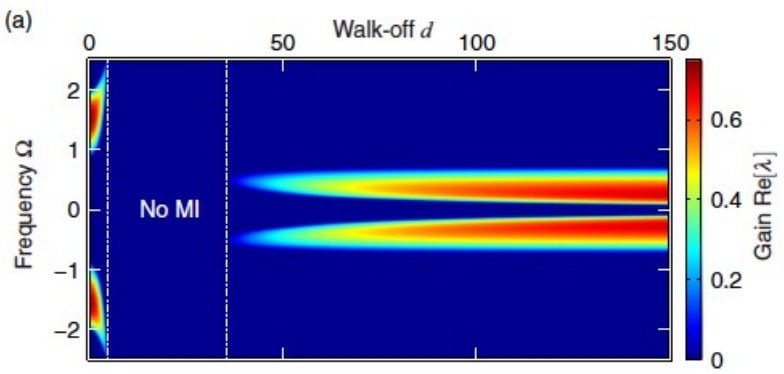

Figure 7. MI gain for a doubly resonant SHG system as a function of frequency and walk-off.[17]

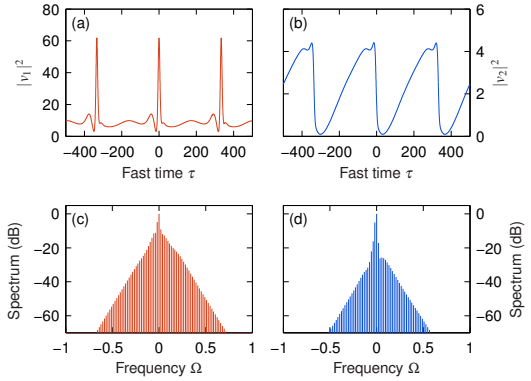

Figure 8. Temporal patterns in a doubly resonant SHG system with large walk-off. (a, b) Temporal profiles at (a) FF and (b) SH wavelengths. Corresponding spectra are shown in (c) and (d), respectively.[17]

In these situation, it is possible to numerically study the dynamics of optical frequency comb generation by means of a map[22] involving the so-called single-envelope equation (SEE)[23–27] for the envelope A^m of the real electric field E. We consider here a waveguide with both quadratic and cubic nonlinearity, i.e., the total nonlinear polarization is $P_{NL} = P_{NL}^{(2)} + P_{NL}^{(3)} = \epsilon_0(\chi^{(2)}E^2 + \chi^{(3)}E^3)$, where $\chi^{(2)}$ and $\chi^{(3)}$ are the quadratic and cubic nonlinear susceptibilities, respectively. The map is constructed by combining the SEE with the appropriate boundary conditions,[7,8] viz.

$$\mathscr{F}\left[A^{m+1}(\tau,0)\right] = \sqrt{\hat{\theta}(\Omega)}\mathscr{F}\left[A_{\rm in}\right] + \sqrt{1-\hat{\theta}(\Omega)}e^{i\phi_0}\mathscr{F}\left[A^m(\tau,L)\right], \tag{11}$$

$$\left[\partial_z - iD\left(i\frac{\partial}{\partial\tau}\right) + \frac{\alpha_d}{2}\right]A^m(\tau,z) = i\rho_0\left(1 + i\tau_{sh}\frac{\partial}{\partial\tau}\right)p_{NL}(\tau,z,A^m), \tag{12}$$

where p_{NL} is the broadband envelope of the nonlinear polarization P_{NL}. Eq. (11) is written in the Fourier domain, to take into account the frequency-dependent transmission coefficient $\hat{\theta}(\Omega)$. Here $\Omega = \omega - \omega_0$, and ω_0 is a reference frequency (which is set to coincide with the driving pump frequency). Eq. (11) is the boundary condition that determines the intra-cavity field $A^{m+1}(\tau, z = 0)$ at the beginning of roundtrip $m + 1$ in terms of the field from the end of the previous roundtrip $A^m(\tau, z = L)$ and the pump field $A_{\rm in}$. The SEE (12) is, as before, written in a reference frame moving at the group velocity at ω_0. Moreover, $\rho_0 = \omega_0/(2n_0c\epsilon_0)$, where $n_0 = n(\omega_0)$ is the linear refractive index at ω_0, $\tau_{sh} = 1/\omega_0$ is the shock coefficient that describes the frequency dependence of the nonlinearity,[23] and α_d is the distributed linear loss coefficient. In Eq. (12) the nonlinear polarization p_{NL}

is given by the sum of the quadratic and cubic contributions[24–27]

$$p_{NL}^{(2)} = \frac{\epsilon_0 \chi^{(2)}}{2} \left[2|A|^2 \exp(i\psi(t,z)) + A^2 \exp(-i\psi(\tau,z)) \right], \tag{13}$$

$$p_{NL}^{(3)} = \frac{\epsilon_0 \chi^{(3)}}{4} \left[3|A|^2 A + A^3 \exp(-2i\psi(\tau,z)) \right]. \tag{14}$$

Here the round-trip index m is omitted for simplicity of notation; moreover, $|A|^2$ only contains non-negative frequency $\omega_0 \geq 0$ components,[24,25] and $\psi(\tau,z) = \omega_0\tau - (\beta_0 - \beta_1\omega_0)z$. The quadratic nonlinear coefficient $d\,[\mathrm{m}/\sqrt{\mathrm{W}}] = \chi^{(2)}/2$, and the nonlinear refractive index $n_2 = 3\chi^{(3)}/(8n_0)$. In Eq. (18) we did not include Raman scattering: the role of Raman scattering on optical frequency comb generation will be briefly discussed in the next section, dealing with silicon microresonators. The real electric field is obtained as $E(\tau,z) = (A(\tau,z)\exp\{i\left[\beta_0 - \beta_1\omega_0\right]z - i\omega_0\tau\} + c.c.)/2$, and the total nonlinear polarization reads as

$$P_{NL}(\tau,z) = (p_{NL}(\tau,z)\exp\{i\left[\beta_0 - \beta_1\omega_0\right]z - i\omega_0\tau\} + c.c.)/2. \tag{15}$$

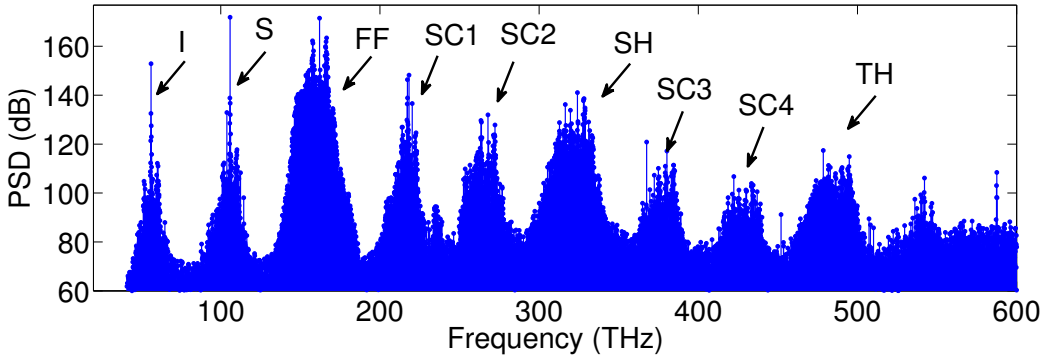

Figure 9. Broadband intra-cavity spectrum with CW pump at 1850 nm and power $P_{\mathrm{in}} = 100\,\mathrm{mW}$ at 1600 round-trips.[21]

In Fig. 9 we show an example of a numerical simulation using the map of Eqs. (11)-(12) for describing optical frequency combs resulting from a non-degenerate OPO process in a radially poled lithium niobate microresonator, with the CW pump power $P_{\mathrm{in}} = 100$ mW.[21] The resulting broadband intra-cavity power spectral density shown in Fig. 9 shows that, in addition to FF, SH and third-harmonic (TH) combs, two additional combs are generated around signal and idler frequencies. Fig. 9 also shows the presence of several secondary combs between the FF and the SH, and between the SH and the TH, respectively. These combs are generated by sum-frequency generation (SFG) and difference frequency generation (DFG) processes. Overall, Fig. 9 shows that a quadratic microresonator may be used to generate a multi-comb array extending from the mid-infrared (MIR) into the ultraviolet with a spacing of a single FSR. For example, consider SFG between the FF (SH) and the idler: this process leads to secondary comb SC1 (SC3) centered at $f_{\mathrm{SC1}} = f_{\mathrm{FF}} + f_{\mathrm{I}} \simeq 218\,\mathrm{THz}$ ($f_{\mathrm{SC3}} = f_{\mathrm{SH}} + f_{\mathrm{I}} \simeq 380\,\mathrm{THz}$). On the other hand, DFG between the SH (TH) and the idler leads to a secondary comb SC2 (SC4) which is centered at $f_{\mathrm{SC2}} = f_{\mathrm{SH}} - f_{\mathrm{I}} \simeq 268\,\mathrm{THz}$ ($f_{\mathrm{SC4}} = f_{\mathrm{TH}} - f_{\mathrm{I}} \simeq 430\,\mathrm{THz}$).

5. SEMICONDUCTOR MICRORESONATOR COMBS

The large Kerr nonlinearity and the potential for fully integrated photonics circuits makes silicon microresonators important candidates for implementing optical frequency comb sources. On the other hand, the presence of nonlinear losses owing to multiphoton absorption processes should be properly taken into account in the modelling of these devices. Quite importantly, the loss resulting from free carriers can be mitigated by suitably controlling the free carrier lifetime (FCT). The nonlinear dynamics of frequency comb generation in silicon microresonators may be described in terms of a cavity averaged SEE for the field envelope A, which includes linear loss and

dispersion, the Kerr effect, Raman scattering, two-photon absorption (TPA), three-photon absorption (3PA), free carrier absorption (FCA), and free carrier dispersion (FCD)[28–32]

$$\left[\frac{1}{v_g}\partial_t - iD + \alpha + i\delta + \frac{\sigma}{2}(1+i\mu)\langle N_c(t)\rangle\right] A(t,\tau) = f_0 + ik_0\left(1 + i\tau_{sh}\frac{\partial}{\partial\tau}\right) p_{NL}^{(3)}(t,\tau) \tag{16}$$

coupled with the evolution equation for the averaged carrier density $\langle N_c(t)\rangle$

$$\partial_t \langle N_c(t)\rangle = \frac{\beta_{TPA}(\omega)}{2\hbar\omega_0}\langle |A|^4\rangle + \frac{\gamma_{3PA}}{3\hbar\omega_0}\langle |A|^6\rangle - \frac{\langle N_c(t)\rangle}{\tau_{eff}} \tag{17}$$

where $v_g = c/n_g$ and n_g are the group velocity and index at the pump carrier frequency ω_0, $k_0 = \omega_0/c$, and $\tau_{sh} = 1/\omega_0$. In Eq.(17), brackets denote average over the cavity circulation time t_R: $\langle X(t)\rangle = (1/t_R)\int_{-\tau_r/2}^{\tau_r/2} X(\tau,t)d\tau$, so that Eq.(17) describes the buildup of carriers within the cavity over many round trips, supposing that the FCT $\tau_{eff} \gg t_R$.

In Eq.(16) the linear loss coefficient $\alpha = \alpha'/L$ with $\alpha' = \alpha_i L + \theta/2$. Moreover σ is the FCA coefficient, μ is the FCD coefficient, β_{TPA} is the TPA coefficient, $f_0 = (\sqrt{\theta}/L)A_{in}$ and A_{in} is the injected CW pump amplitude. The nonlinear polarization reads as

$$p_{NL}^{(3)} = n_2[(1-\gamma_R)(\eta \otimes (|A|^2 A) + ir_3|A|^4 A + A^3\exp(-2i\omega_0\tau)/3) + \gamma_R\int_{-\infty}^{\tau} h_R(\tau-\tau')|A(\tau')|^2 d\tau']. \tag{18}$$

Here $\otimes$ denotes convolution product, n_2 is the nonlinear index and γ_R is the Raman fraction coefficient associated with the response function

$$h_R(\tau) = H(t)\frac{\tau_1^2+\tau_2^2}{\tau_1\tau_2^2}\exp(-\tau/\tau_2)\sin(\tau/\tau_1), \tag{19}$$

where $H(\tau)$ is the Heaviside function, $\tau_1 = 10.2$ fs and $\tau_2 = 3.03$ ps. For the transverse electric (TE) mode, the scalar Raman gain coefficient is $\gamma_R = g_R\Gamma_R/(n_2 k_0 \Omega_R) = 0.018$, where we used $n_2 = 9\times10^{-18}\mathrm{m}^2/\mathrm{W}$, and the peak parallel Raman gain value $g_R = 2\times10^{-10}\mathrm{m/W}$ at the wavelength $\lambda_0 = 1.55\,\mu$m, the gain bandwidth $\Gamma_R/\pi = 105$ GHz and the peak gain frequency shift $\Omega_R/2\pi = 15.6$ THz. Whereas for the transverse magnetic (TM) mode the parallel Raman gain vanishes in silicon,[30] hence $\gamma_R = 0$.

After a first step involving the design of the spatial mode properties of the silicon microrings, we numerically simulate the temporal dynamics of MIR frequency comb generation by solving Eqs.(16)-(19) in the frequency domain as a set of coupled ordinary differential equations for the resonator modes, with computationally efficient evaluation of the four-wave mixing terms in the time domain via the fast Fourier transform routine.[33] With this approach, we are also able to include in our modelling the frequency dependence of the nonlinear loss terms, such as TPA, as well as of the effective mode area. We used a quantum noise input (one photon per mode), and considered a microresonator with quality factor $Q = \pi n_g/\alpha'\lambda_0 = 3.5\times10^5$ in the critical-coupling regime, i.e., we set $\alpha' = \theta = 2\alpha_d L$, so that $\theta = 0.004$ at $\lambda_0 = 2.6\,\mu$m. We pumped the microring with $P_{in} = 1$ W of input CW power, and used $\sigma = 3.7\times10^{-21}\mathrm{m}^2$, $\mu = 4.7$ and $\gamma_{3PA} = 0.025\,\mathrm{cm}^3/\mathrm{GW}^2$.[34,35]

Consider first the case of pumping the TM mode of a microring with FSR=261 GHz at $\lambda_0 = 2.6\,\mu\mathrm{m}^2$, and no cavity detuning, i.e., $\delta = 0$. Fig.10(a) shows the temporal evolution of the intracavity intensity, corresponding to the generation of a stable cavity soliton pattern.[32] The spectral intensity in Fig.10(b) shows that a transient primary frequency comb is followed, after about 1 ns, by the generation of the soliton comb. It is important

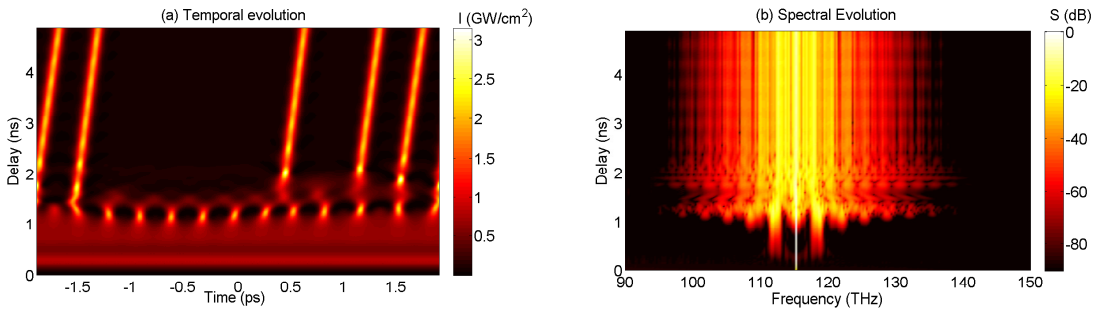

Figure 10. Soliton frequency comb generation from the TM mode of a silicon microring: (a) temporal evolution; (b) spectral evolution of intracavity intensity; Here $\tau_{eff} = 320$ ps and $\lambda_0 = 2.6\,\mu$m[32]

.

to note that, in order to arrive to a stable soliton comb, it is necessary to properly adjust the FCT (here $\tau_{eff} = 320$ ps). This can be achieved, e.g., by tuning the reverse bias voltage applied to a PIN structure embedding the microring.[36,37] Here the mechanism for soliton comb generation in a silicon microring as shown in Fig.10(b) is, first, the noise-induced MI of the CW cavity solution, followed by the development of a self-induced nonlinear cavity detuning introduced by FCD.[32]

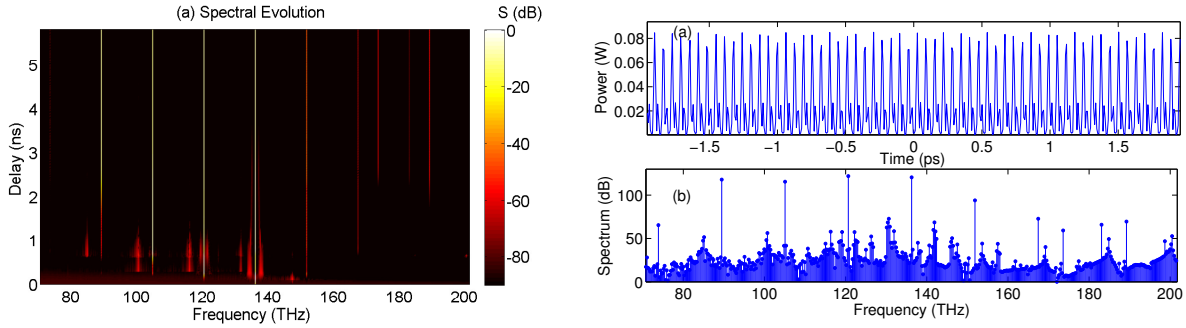

Figure 11. Left: Raman frequency comb from TE mode of silicon microring. Here $\tau_{eff} = 100$ ps and $\lambda_0 = 2.2\,\mu$m; (a) power and (b) spectral profile.[32]

On the other hand, when pumping the TE mode of a silicon microring, one mainly observes the generation of Raman frequency combs.[32] Fig.11 shows that a Raman frequency comb is generated, including three cascaded Raman Stokes lines of nearly equal intensity as the pump wave, as well as three anti-Stokes comb lines and a weaker fourth Stokes line at about 70 THz, for an octave-spanning Raman comb bandwidth in excess of 100 THz. Fig.11 also shows that the Raman comb is associated with a periodic train of pulses of about 15 fs duration.

6. CONCLUSIONS

We have presented an overview of various time domain models for describing optical frequency comb generation in both cubic and quadratic nonlinear cavities. These models involve either a map or a cavity-averaged equation for the recirculating optical field. Cavity averaged models permit to numerically reproduce the properties of experimentally generated optical frequency combs in many practical situations. However we have pointed out that the more general map exhibits multi-valued stationary states, additional bands of MI and novel types of super cavity soliton solutions at high intracavity powers..

In singly or doubly resonant intracavity SH generation, modelling can be simplified by arriving to a single mean-field equation, exhibiting a non-instantaneous cubic nonlinear response function. In all cases, the walk-off between the FF and SH field plays a key role in the nonlinear comb generation dynamics, and only for a sufficiently large walk-off is there sufficient gain to sustain a stable frequency comb at the FF.

In the most general situation when multiple phase matched processes are involved, it proves convenient to instead employ a single envelope equation approach to numerically simulate the process of optical frequency comb generation in the presence of simultaneous nonlinearities. When considering semiconductor microresonator frequency comb sources, multiphoton absorption processes also play a key role, and their control is found to be critical for generating stable soliton frequency combs. Finally, we have shown an example of how Raman scattering may also be exploited for multi-octave spanning optical frequency comb sources based on silicon microring resonators.

ACKNOWLEDGMENTS

This work was funded by the Italian Ministry of University and Research (MIUR) (PRIN 2015KEZNYM (NEMO) and Progetto Premiale QUANTOM - Quantum Opto-Mechanics), the Rutherford Discovery Fellowships of the Royal Society of New Zealand and the Marsden Fund of the Royal Society of New Zealand.

REFERENCES

[1] Del'Haye, P., Schliesser, A., Arcizet, O., Wilken, T., Holzwarth, R., and Kippenberg, T. J., "Optical frequency comb generation from a monolithic microresonator," *Nature* **450**, 1214–1217 (2007).

[2] Kippenberg, T. J., Holzwarth, R., and Diddams, S. A., "Microresonator-based optical frequency combs," *Science* **332**, 555–559 (2011).

[3] Okawachi, Y., Saha, K., Levy, J. S., Wen, Y. H., Lipson, M., and Gaeta, A. L., "Octave-spanning frequency comb generation in a silicon nitride chip," *Optics Letters* **36**, 3398–3400 (2011).

[4] Herr, T., Hartinger, K., and Riemensberger, J., "Universal formation dynamics and noise of Kerr-frequency combs in microresonators," *Nature Photonics* **6**, 480–487 (2012).

[5] Ricciardi, I., Mosca, S., Parisi, M., Maddaloni, P., Santamaria, L., De Natale, P., and De Rosa, M., "Frequency comb generation in quadratic nonlinear media," *Phys. Rev. A* **91**, 063839 (June 2015).

[6] Mosca, S., Ricciardi, I., Parisi, M., Maddaloni, P., Santamaria, L., De Natale, P., and De Rosa, M., "Direct generation of optical frequency combs in (2) nonlinear cavities," *Nanophotonics* **5**(2), 316 (2016).

[7] Haelterman, M., Trillo, S., and Wabnitz, S., "Dissipative modulation instability in a nonlinear dispersive ring cavity," *Optics Communications* **91**(5-6), 401–407 (1992).

[8] Coen, S., Randle, H. G., Sylvestre, T., and Erkintalo, M., "Modeling of octave-spanning Kerr frequency combs using a generalized mean-field Lugiato–Lefever model," *Optics Letters* **38**(1), 37–39 (2013).

[9] Lugiato, L. A. and Lefever, R., "Spatial dissipative structures in passive optical systems," *Physical Review Letters* **58**, 2209–2211 (May 1987).

[10] Leo, F., Coen, S., Kockaert, P., Gorza, S.-P., Emplit, P., and Haelterman, M., "Temporal cavity solitons in one-dimensional Kerr media as bits in an all-optical buffer," *Nature Photonics* **4**, 471–476 (May 2010).

[11] Hansson, T. and Wabnitz, S., "Frequency comb generation beyond the Lugiato–Lefever equation: multi-stability and super cavity solitons," *Journal of the Optical Society of America B* **32**, 1259–1266 (July 2015).

[12] Hansson, T., Modotto, D., and Wabnitz, S., "Dynamics of the modulational instability in microresonator frequency combs," *Phys. Rev. A* **88**, 023819 (Aug. 2013).

[13] Wabnitz, S., "Suppression of interactions in a phase-locked soliton optical memory," *Optics Letters* **18**(8), 601–603 (1993).

[14] Coen, S. and Haelterman, M., "Modulational instability induced by cavity boundary conditions in a normally dispersive optical fiber," *Physical Review Letters* **79**(21), 4139–4142 (1997).

[15] Buryak, A. V., Trapani, P. D., Skryabin, D. V., and Trillo, S., "Optical solitons due to quadratic nonlinearities: from basic physics to futuristic applications," *Phys. Rep.* **370**(2), 63–235 (2002).

[16] Leo, F., Hansson, T., Ricciardi, I., De Rosa, M., Coen, S., Wabnitz, S., and Erkintalo, M., "Walk-Off-Induced Modulation Instability, Temporal Pattern Formation, and Frequency Comb Generation in Cavity-Enhanced Second-Harmonic Generation," *Phys. Rev. Lett.* **116**, 033901 (Jan. 2016).

[17] Leo, F., Hansson, T., Ricciardi, I., De Rosa, M., Coen, S., Wabnitz, S., and Erkintalo, M., "Frequency-comb formation in doubly resonant second-harmonic generation," *Phys. Rev. A* **93**, 043831 (2016).

[18] Hansson, T., Leo, F., Erkintalo, M., Coen, S., Ricciardi, I., De Rosa, M., and Wabnitz, S., "Singly resonant second-harmonic-generation frequency-combs," *Phys. Rev. A* **95**, 013805 (2017).

[19] Stolen, R. H., Tomlinson, W. J., Haus, H. A., and Gordon, J. P., "Raman response function of silica-core fibers," *J. Opt. Soc. Am. B* **6**(6), 1159–1166 (1989).

[20] Conti, C., Schmidt, M. A., Russell, P. S. J., and Biancalana, F., "Highly Noninstantaneous Solitons in Liquid-Core Photonic Crystal Fibers," *Phys. Rev. Lett.* **105**, 263902 (Dec. 2010).

[21] Hansson, T., Leo, F., Erkintalo, M., Anthony, J., Coen, S., Ricciardi, I., De Rosa, M., and Wabnitz, S., "Single envelope equation modeling of multi-octave comb arrays in microresonators with quadratic and cubic nonlinearities," *J. Opt. Soc. Am. B* **33**, 1207 (June 2016).

[22] Ikeda, K., "Multiple-valued stationary state and its instability of the transmitted light by a ring cavity system," *Optics Communications* **30**(2), 257–261 (1979).

[23] Genty, G., Kinsler, P., Kibler, B., and Dudley, J. M., "Nonlinear envelope equation modeling of sub-cycle dynamics and harmonic generation in nonlinear waveguides," *Optics Express* **15**, 5382 (2007).

[24] Conforti, M., Baronio, F., and De Angelis, C., "Nonlinear envelope equation for broadband optical pulses in quadratic media," *Physical Review A* **81**, 053841 (2010).

[25] Conforti, M., Baronio, F., and De Angelis, C., "Ultrabroadband optical phenomena in quadratic nonlinear media," *IEEE Photonics Journal* **2**, 600–610 (2010).

[26] Kozlov, V. and Wabnitz, S., "Harmonic and supercontinuum generation in quadratic and cubic nonlinear optical media," *Journal of the Optical Society of America B* **27**, 1707–1711 (2010).

[27] Baronio, F., Conforti, M., De Angelis, C., Modotto, D., Wabnitz, S., Andreana, M., Tonello, A., Leproux, P., and Couderc, V., "Second and third order susceptibilities mixing for supercontinuum generation and shaping," *Optical Fiber Technology* **18**, 283–289 (2012).

[28] Lau, R. K. W., Lamont, M. R. E., Okawachi, Y., and Gaeta, A. L., "Effects of multiphoton absorption on parametric comb generation in silicon microresonators," *Optics Letters* **40**, 2778 (June 2015).

[29] Lamont, M., Okawaki, Y., and Gaeta, A., "Route to stabilized ultrabroadband microresonator-based frequency combs," *Opt. Lett.* **38**, 3478 (2013).

[30] Lin, Q., Painter, O., and Agrawal, G., "Nonlinear optical phenomena in silicon waveguides: modeling and applications," *Opt. Express* **25**, 16604–16644 (2007).

[31] Yin, L. and Agrawal, G., "Impact of two-photon absorption on self-phase modulation in silicon waveguides," *Opt. Lett.* **32**, 2031 (2007).

[32] Hansson, T., Modotto, D., and Wabnitz, S., "Mid-infrared soliton and Raman frequency comb generation in silicon microrings," *Optics Letters* **39**, 6747 (Dec. 2014).

[33] Hansson, T., Modotto, D., and Wabnitz, S., "On the numerical simulation of Kerr frequency combs using coupled mode equations," *Optics Communications* **312**, 134–136 (2014).

[34] Lau, R., Lamont, M., Griffith, A., Okawachi, Y., Lipson, M., and Gaeta, A., "Octave-spanning mid-infrared supercontinuum generation in silicon nanowaveguides," *Opt. Lett.* **39**, 4518 (2014).

[35] Wang, T., Venkatram, N., Gosciniak, J., Cui, Y., Qian, G., Li, W., , and Tan, D., "Multi-photon absorption and third-order nonlinearity in silicon at mid-infrared wavelengths," *Opt. Express* **21**, 32192 (2013).

[36] Griffith, A. G., Lau, R. K., Cardenas, J., Okawachi, Y., Mohanty, A., Fain, R., Lee, Y. H. D., Yu, M., Phare, C. T., Poitras, C. B., Gaeta, A. L., and Lipson, M., "Silicon-chip mid-infrared frequency comb generation," *Nature Communications* **6**, 6299 (Feb. 2015).

[37] Turner-Foster, A., Foster, M., Levy, J., Poitras, C., Salem, R., Gaeta, A., and Lipson, M., "Ultrashort free-carrier lifetime in low-loss silicon nanowaveguides," *Opt. Express* **18**, 3582–3591 (2010).